Momentum Distribution in the Unitary Bose Gas from First Principles

Tommaso Comparin* and Werner Krauth†
Laboratoire de Physique Statistique, École Normale Supérieure/PSL Research University, UPMC, Université Paris Diderot, CNRS, 24 rue Lhomond, 75005 Paris, France
(Received 24 May 2016; published 22 November 2016)

We consider a realistic bosonic N-particle model with unitary interactions relevant for Efimov physics. Using quantum Monte Carlo methods, we find that the critical temperature for Bose-Einstein condensation is decreased with respect to the ideal Bose gas. We also determine the full momentum distribution of the gas, including its universal asymptotic behavior, and compare this crucial observable to recent experimental data. Similar to the experiments with different atomic species, differentiated solely by a three-body length scale, our model only depends on a single parameter. We establish a weak influence of this parameter on physical observables. In current experiments, the thermodynamic instability of our model from the atomic gas towards an Efimov liquid could be masked by the dynamical instability due to three-body losses.

DOI: 10.1103/PhysRevLett.117.225301

First predicted in 1970 [1], the Efimov effect describes the behavior of three strongly interacting bosons when any two of them cannot bind. At unitarity, when the scattering length diverges, the three-body bound states are scale invariant and they form a sequence up to vanishing binding energy and infinite spatial extension. Efimov trimers had been intensely discussed in nuclear physics, but it was in an ultracold gas of caesium atoms that they were finally discovered [2]. To observe Efimov trimers, experiments in atomic physics rely on Feshbach resonances [3], which allow one to instantly switch a gas between weak interactions and the unitary limit. Such a control of interactions is lacking in nuclear physics or condensed matter experiments, and singular interactions can be probed there only in the presence of accidental fine tuning [4]. Beyond the original system [2], Efimov trimers have now been observed for several multicomponent systems, including bosonic, fermionic, and Bose-Fermi mixtures [5–7]. These experimental findings are interpreted in terms of the theory of few-body strongly interacting quantum systems. For three identical bosons in three dimensions, a complete universal theory is available, on and off unitarity [4]. Further theoretical work is aimed at understanding bound states for more than three bosons, mixtures, and the effects of dimensionality.

Near-unitary interparticle interactions also impact the thermodynamics of the atomic gas, the description of which presents a challenge beyond the traditional theory of the Efimov effect. In addition, mean-field theory does not apply to infinite interactions [8], and the virial expansion [9] fails to describe the low-temperature state. Moreover, in atomic-physics experiments, strong interactions enhance the three-body loss rate, making the gas of bosons unstable. A characterization of the universal dynamics of these losses has been recently achieved [10–12]. On the other hand, a single breakthrough experiment [13] has addressed the low-temperature thermodynamics for a unitary bosonic gas, coming to the conclusion that equilibrium was approached faster than the system lifetime. The importance of this system stems from its universal character: All differences between atomic species may be encoded in a single three-body parameter, related to the van der Waals length [14]. However, this prominent experiment could not be interpreted univocally, as first-principles theoretical predictions were lacking. In the present work, we obtain these predictions for a model which shares the experimental system's universality. We develop a novel quantum Monte Carlo algorithm [15] that overcomes the peculiar challenges posed by the infinite interactions. This allows us to compute the critical temperature for Bose-Einstein condensation, and the full momentum distribution $n(\mathbf{k})$ throughout the entire phase diagram, including its universal asymptotic behavior.

In the unitary limit, the scattering length diverges, and atomic pair interactions are powerful yet very short-ranged. The bosonic pair correlation function $g^{(2)}(\mathbf{r})$ diverges as $1/r^2$ at short distances $r = |\mathbf{r}|$, yet two isolated unitary bosons barely hold together: They form a molecule of infinite radius and vanishing binding energy. In thermodynamic equilibrium, three or more such bosons, with zero-range interactions, collapse into a single point, unless the unitary pair interactions are counterbalanced by a three-body repulsion. In experimental systems the latter is effectively realized by the van der Waals potential [14], so that the unitary Bose gas is stabilized against collapse. The divergence of $g^{(2)}(\mathbf{r})$ persists in the gas, with a finite contact density $c_2 = \lim_{r\to 0}(4\pi r)^2 g^{(2)}(\mathbf{r})$. The large-$k$ asymptotics of the momentum distribution [16,17] is governed by Tan's contact parameter $C_2 = c_2 V$ (where V is the system volume), and it decays as $n(\mathbf{k}) \simeq C_2/k^4$ for $k \to \infty$.

We consider N bosons at temperature T in a periodic cubic box (thermodynamic NVT ensemble). Pair interactions are

of zero range and infinite depth, and the resonant two-body bound state realizes an infinite scattering length. In addition, any three particles a, b, c are subject to a hard cutoff $R > R_0$ on their hyperradius R, defined as the mean of their squared pair distances: $R^2 \equiv (r_{ab}^2 + r_{bc}^2 + r_{ac}^2)/3$. This realistic model describes ultracold atomic ensembles with an interaction range much smaller than the scattering length, the interparticle distance, and the thermal de Broglie wavelength. The two-body interactions, with their infinite scattering length, provide no scale. The model's phase diagram thus depends on two dimensionless numbers, namely, the thermal de Broglie wavelength $\lambda_{\rm th}\rho^{1/3}$, and the three-body cutoff $R_0\rho^{1/3}$, both in units of the typical interparticle distance $\rho^{-1/3}$ [where $\lambda_{\rm th} = \sqrt{2\pi\hbar^2\beta/m}$, $\beta = 1/(k_B T)$, and $\rho = N/V$]. At high temperature, three-particle effects are suppressed, and the model depends only on $\lambda_{\rm th}\rho^{1/3}$. In experiments at low temperature, three-body correlations lead to strong recombination losses, with a loss rate scaling as $\sim T^{-2}$ [10–12], the predominant source of instability of the system. In contrast, our model conserves particle number.

Path-integral quantum Monte Carlo techniques allow us to solve this model from first principles, that is, without systematic errors. Computational challenges are posed by the divergence of $g^{(2)}(\mathbf{r})$ at contact [see Fig. 1(b)] and by the need to determine $n(\mathbf{k})$ for large momenta k [see Fig. 1(d)]. This corresponds to computing the single-particle correlation function $g^{(1)}(\mathbf{r})$—the inverse Fourier transform of $n(\mathbf{k})$—at small r, close to its cusp singularity at $r \to 0$ [see Fig. 1(c)]. Our path-integral quantum Monte Carlo algorithm [15,18–20] samples both closed and open path-integral configurations [cf. Fig. 1(a)]. The former give access to the superfluid fraction ρ_s/ρ (via the winding-number estimator [21]) and to the pair-correlation function $g^{(2)}(\mathbf{r})$ (from which we extract the contact density c_2). Open configurations, in contrast, sample the single-particle correlation function $g^{(1)}(\mathbf{r})$, and give access to the normalized momentum distribution [satisfying $\int d\mathbf{k} n(\mathbf{k})/(2\pi)^3 = N$ in the normal gas]. A dedicated estimator allows us to sample $n(\mathbf{k})$ for arbitrarily large momenta k [cf. Supplemental Material (i) [22]].

We include zero-range unitary interactions between two bosons through the exact two-body propagator [23,24], and treat them with a highly efficient direct-sampling approach [15]. The many-body density matrix is then built via the pair-product approximation. The hyperradial cutoff is included via the Trotter breakup [18], and an effective value of R_0 is obtained—for a finite imaginary-time discretization—through the comparison with the expression for the hyperradial wave function of a single universal trimer [15,23]. For three unitary bosons, the length scale R_0 sets a lower bound on the Efimov energy spectrum, and specifies a three-body ground state. At low temperature, our Monte Carlo simulations for $N = 3$ allow us to obtain excellent agreement of the hyperradial probability

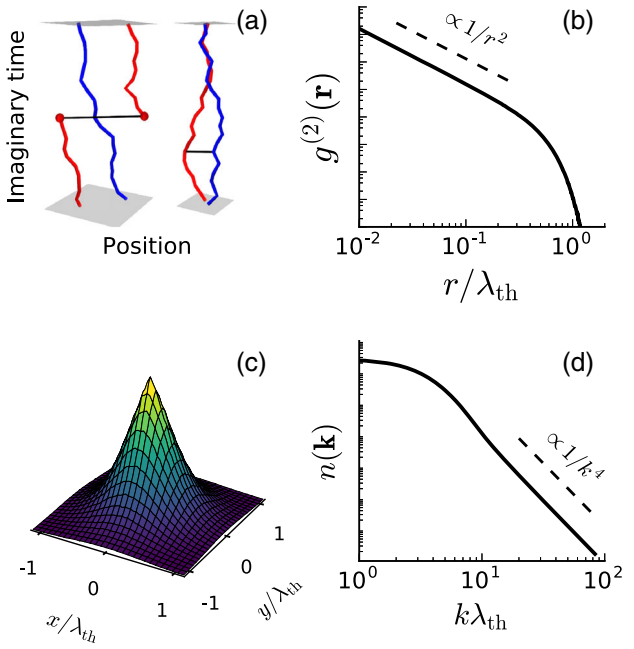

FIG. 1. Correlation functions for two unitary bosons. (a) Open (left) and closed (right) co-cyclic configurations in the path-integral representation. Closed configurations yield $g^{(2)}(\mathbf{r})$. Open configurations yield $n(\mathbf{k})$ and its inverse Fourier transform $g^{(1)}(\mathbf{r})$. (b) Pair-correlation function $g^{(2)}(\mathbf{r})$ (distance distribution in closed configurations), featuring a r^{-2} divergence at small r. (c) Cut of $g^{(1)}(\mathbf{r})$ (distribution of the distance between open ends), for $\mathbf{r} = (x, y, 0)$, illustrating the cusp at $\mathbf{r} \simeq 0$. (d) Momentum distribution $n(\mathbf{k})$ with asymptotic decay, $\propto 1/k^4$, at large $\mathbf{k}$.

distribution and the momentum distribution for our model with the corresponding quantities for the universal Efimov trimer [4,25] [see Fig. 2(a) and Fig. 2(b)], providing also a parameter-free check of our computer program.

In the thermodynamic NVT ensemble, unitary bosons phase separate below a given temperature into a normal or Bose-Einstein-condensed gas dominated by entropy and a high-density Efimov liquid of low potential energy

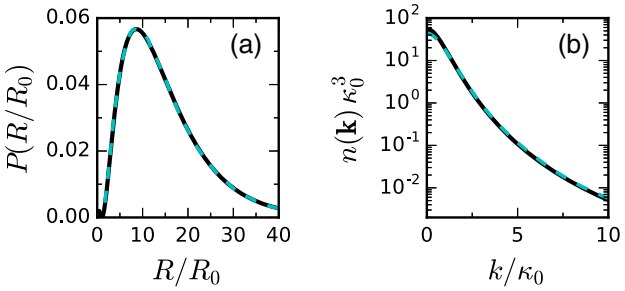

FIG. 2. Correlation functions for three unitary bosons. (a) Hyperradial probability distribution for three co-cyclical bosons with hyperradial cutoff at low temperature (cyan dashed line) and for the universal Efimov trimer (black solid line, from Ref. [4]). (b) Momentum distribution for three co-cyclical bosons (cyan dashed line), and for the universal trimer (black solid line, from Ref. [25]), in units of the trimer binding momentum κ_0.

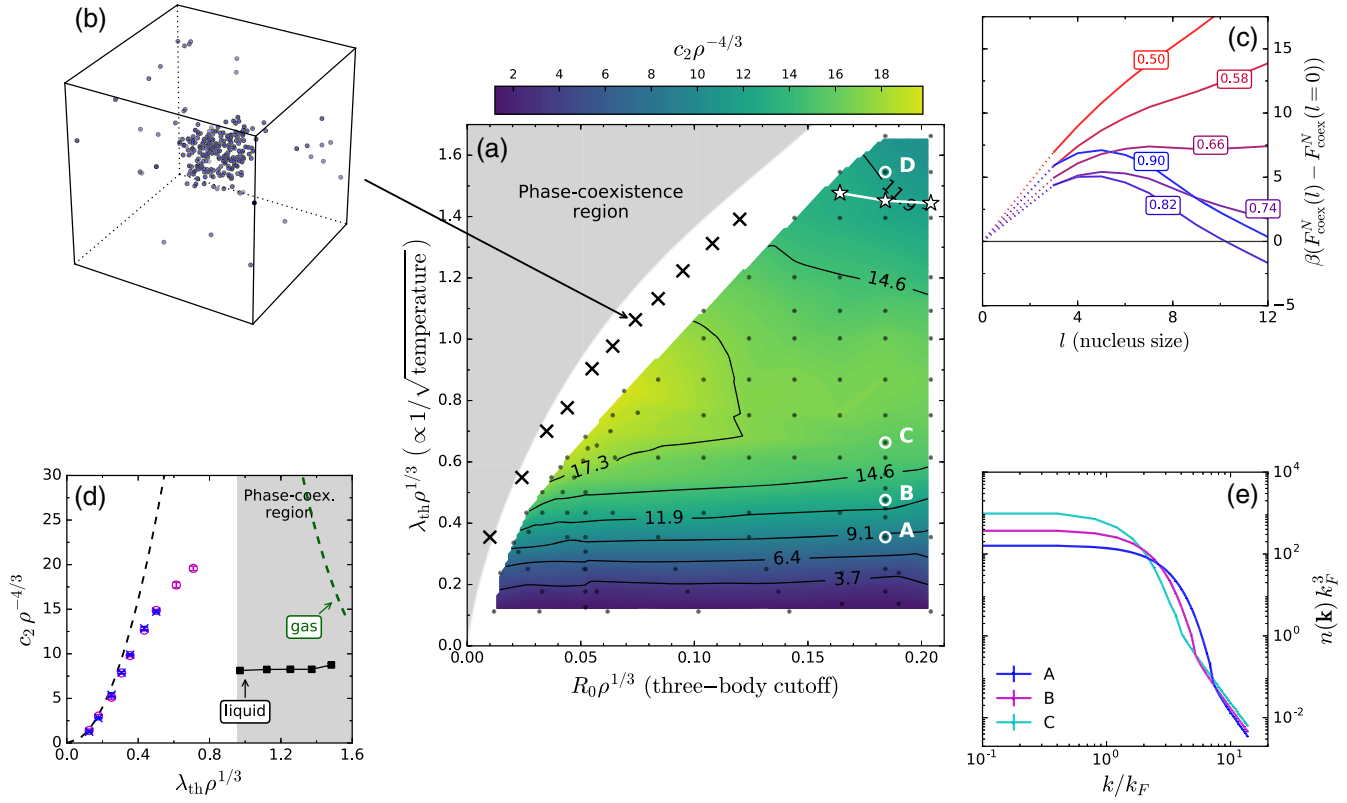

FIG. 3. Equilibrium phase diagram of unitary bosons. (a) Contact density $c_2\rho^{-4/3}$, as a linear interpolation of numerical results [extracted from $g^{(2)}(\mathbf{r})$, for $N = 64$]. White stars: transition between normal gas and superfluid (Bose-Einstein condensed) phase. Black crosses: Phase-separated points. Gray area: Phase-coexistence region [23]. (b) Stable Efimov-liquid droplet coexisting with a normal gas ($N = 256$). (c) Excitation free energy for the Efimov-liquid nucleation, vs nucleus size l. $\lambda_{\rm th}\rho^{1/3}$ varies between lines (see labels), between 0.5 (monotonically increasing, red line) and 0.9 (barrier, blue line). The hyperradial cutoff is fixed ($R_0\rho^{1/3} = 0.03$), and the phase-separation region sets in at $\lambda_{\rm th}\rho^{1/3} \simeq 0.66$. (d) Contact density $c_2\rho^{-4/3}$ vs $\lambda_{\rm th}\rho^{1/3}$, for $R_0\rho^{1/3} = 0.052$: Virial expansion (black dashed line) and numerical results, via the $n(\mathbf{k})$ and $g^{(2)}(\mathbf{r})$ estimators (crosses, circles). In the phase-coexistence region, the liquid and gas phases have different contact densities (for the gas, the virial expansion is used). (e) Momentum distribution [in units of the Fermi momentum $k_F = (6\pi^2\rho)^{1/3}$] for parameters corresponding to points A, B, and C, in panel (a).

(see Fig. 3(a) and Ref. [23]). An equilibrium liquid bubble forms inside the gas [Fig. 3(b)], and the nucleation process is reversible across the coexistence line. For $R_0 \to 0$, the gas-to-liquid condensation energy $\propto 1/R_0^2$ overcomes the gas entropy loss at arbitrarily high temperatures, so that the coexistence line starts at $\lambda_{\rm th}\rho^{1/3} = R_0\rho^{1/3} = 0$. In the phase-coexistence region, the free energy $F^N_{\rm coex}(l)$ is composed of two terms, corresponding to the Efimov-liquid nucleus of l particles and to the gas of the remaining $N - l$ particles. An analytical model, based on the virial expansion of the gas [9] and the known ground-state energies for small Efimov-liquid nuclei [26] (supposed incompressible), allows us to model the excitation free energy [see Supplemental Material (v) [22]]. In the homogeneous gas phase, $F^N_{\rm coex}(l)$ monotonically increases with l [Fig. 3(c)]. At lower temperatures, the gas becomes metastable, with a free-energy barrier at a critical cluster size l^*. The nucleation rate per volume is proportional to $\exp(-\beta\Delta F)$, where $\Delta F = F^N_{\rm coex}(l^*) - F^N_{\rm coex}(0)$ is the free-energy barrier to overcome the critical cluster size l^*. At low temperature, $\beta\Delta F$ and, therefore, the characteristic nucleation time for the Efimov liquid remain finite [see Fig. 3(c)]. The observed long experimental lifetime [13] is consistent with the idea that the phase-separation instability does not take place, in current experiments, as three-body losses effectively destabilize liquid droplets before the critical nucleus size $l^* \simeq 5$ is reached. A study of the many-body quantum dynamics will be needed to confirm this hypothesis.

In the stable region of the phase diagram, the momentum distribution $n(\mathbf{k})$ is, in principle, obtained as the Fourier transform of $g^{(1)}(\mathbf{r})$, the distribution for distance vectors of open configurations [cf. Fig. 1(a)]. This estimator, however, poorly samples the short-distance cusp in $g^{(1)}(\mathbf{r})$ [equivalently, the large-k behavior of $n(\mathbf{k})$]. Our approach is rather based on an average of the analytical two-body expression, to determine $n(\mathbf{k})$ at arbitrarily large k [see Supplemental Material (i) [22]]. The asymptotic behavior of $n(\mathbf{k}) = C_2/k^4$ for $k \to \infty$ is also contained

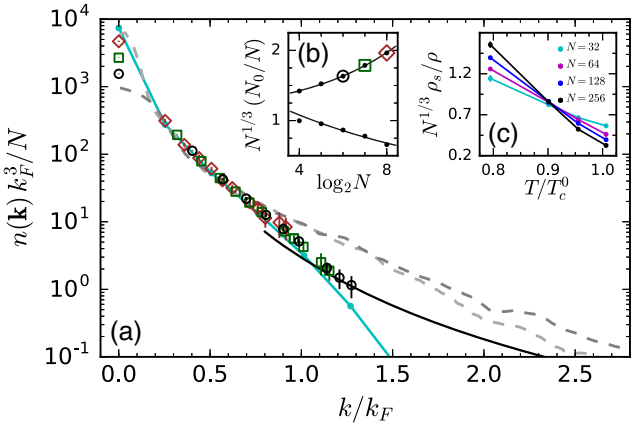

FIG. 4. Full momentum distribution $n(\mathbf{k})$ in the Bose-Einstein-condensed gas phase. (a) $n(\mathbf{k})$ at $\lambda_{\rm th}\rho^{1/3} = 1.545$, $R_0\rho^{1/3} = 0.184$ [point D in Fig. 3(a)]. First-principles results for $N = 64$, 128, and 256 (black circles, green squares, brown diamonds, respectively), and $\propto C_2/k^4$ asymptotic behavior for $k \to \infty$ (for $N = 64$, black solid line). Dashed lines are experimental data of Ref. [13] for two different densities. The momentum distribution for $N = 256$ ideal bosons is also shown (cyan solid line). (b) Scaling of the condensed fraction N_0/N with the system size, in the normal and condensed phases. The upper curve (at $T < T_c$) corresponds to the parameters in panel (a), and the exact numerical data are fitted by $N^{1/3}(N_0/N) \simeq 1.06 + 0.14N^{1/3}$ [same symbols for N as in panel (a)]. The lower curve is at $\lambda_{\rm th}\rho^{1/3} \simeq 1.373$ (corresponding to $T > T_c$), and is fitted by $N^{1/3}(N_0/N) \simeq 1.71N^{-1/6}$. (c) Rescaled superfluid fraction vs temperature, at $R_0\rho^{1/3} = 0.184$. The crossing point at $T/T_c^0 \simeq 0.9$ (corresponding to $\lambda_{\rm th}\rho^{1/3} \simeq 1.45$) shows that T_c is lowered by 10% with respect to the ideal Bose gas, in the limit $N \to \infty$.

in the contact density, obtained from closed-path configurations [see Fig. 3(d)]. In the normal phase, the small-k part of the momentum distribution $n(\mathbf{k})$ resembles the one of ideal bosons: The peak at $k = 0$ corresponds to the Maxwell-Boltzmann distribution $\exp(-\beta k^2/2)$ in the classical limit (at high temperature), and the narrowing at lower temperature is enhanced by bosonic statistics [see Fig. 3(e)]. At large k, $n(\mathbf{k})$ crosses over into the C_2/k^4 asymptotic behavior, with a crossover point which scales as $k/k_F \propto 1/(\lambda_{\rm th}\rho^{1/3})$ for large temperature, where $k_F \equiv (6\pi^2\rho)^{1/3}$ is the Fermi momentum. In the phase-coexistence region, we obtain two different contact densities for the gas and for the Efimov liquid [see Fig. 3(d)].

Throughout the homogeneous region, the momentum distribution only depends weakly on $R_0\rho^{1/3}$, both in the full $n(\mathbf{k})$ and in its asymptotic tail, underlining the generality of the model under study. The slow decrease of c_2 for increasing $R_0\rho^{1/3}$ (absent at high temperature, $\lambda_{\rm th}\rho^{1/3} \to 0$) corresponds to a small suppression of $g^{(2)}(\mathbf{r})$ at short distance, indirectly caused by the hyperradial cutoff. At high temperature, our first-principles results for the contact density rapidly fall below the predictions of the virial expansion [27–29] [Fig. 3(d)], leveling off at intermediate temperature, and finally decreasing at lower temperature. This nonmonotonic behavior was already qualitatively predicted [29]. The low-temperature values of $c_2\rho^{-4/3}$ fall in the same range of previous zero-temperature approximate results [30–32] [cf. Supplemental Material (ii) [22]].

For large three-body cutoff ($R_0\rho^{1/3} \gtrsim 0.16$), the normal gas undergoes Bose-Einstein condensation before phase separation sets in. At finite k, $n(\mathbf{k})$ has very small finite-size effects, making the comparison with experiments feasible. Data for harmonically trapped Rb atoms [13] are available up to $k/k_F \simeq 3$ and they are considered equilibrated for $k/k_F \gtrsim 0.5$. At small k, the harmonic-trap geometry has the strongest influence. Up to momenta $k \approx k_F$, the experimental curves overlap with the theoretical data [see Fig. 4(a)]. As the asymptotic k^{-4} behavior of $n(\mathbf{k})$ sets in for the numerical curve ($k \gtrsim 1.1k_F$, at the chosen temperature), the experimental curve remains higher. This deviation is difficult to reconcile with our model, as the k^{-4} prefactor is expected to decrease even further at lower temperature [see Supplemental Material (ii) [22]].

The condensate fraction is related to the $\mathbf{k} = \mathbf{0}$ component of $n(\mathbf{k})$, $N_0/N = n(\mathbf{k} = \mathbf{0})/(\mathrm{NV})$. Below the critical temperature T_c, it remains nonzero for $N \to \infty$, with finite-size corrections $\propto N^{-1/3}$. In the normal phase, in contrast, the large-N limit of N_0/N vanishes. These two behaviors are clearly distinguished in the data [see Fig. 4(b)]. The scaling of the superfluid fraction yields a precise estimate of the critical temperature [33] [see Fig. 4(c) and Supplemental Material (iii) [22]]. In the unitary Bose gas, T_c is reduced by 10%: The critical value of $\lambda_{\rm th}\rho^{1/3}$ is between 1.44 and 1.48 [see Fig. 3(a)], while the ideal-bosons transition [34] is at $\lambda_{\rm th}\rho^{1/3} \simeq 1.377$. The deviation of T_c from T_c^0 (the ideal-bosons critical temperature) is larger for smaller values of $R_0\rho^{1/3}$. It is instructive to compare $n(\mathbf{k})$ with the ideal-gas curve. Unitary interactions cause a depletion of the condensate, i.e., a decrease of N_0/N. At temperature $T \lesssim T_c$, this follows from the negative shift of the critical temperature, $T_c < T_c^0$. While the $\mathbf{k} = \mathbf{0}$ component of $n(\mathbf{k})$ is smaller, on the other hand, the tail of the distribution is more important [cf. the power-law k^{-4} decay, vs the exponential suppression of $n(\mathbf{k})$ for ideal bosons]. At point D in Fig. 3(a), the depletion of the condensate is not entirely compensated by the large-k contribution [see Supplemental Material (iv) [22]]. This leads to the reweighting of the unitary gas momentum distribution with respect to the one of the ideal Bose gas, without introducing any new features.

Both for three-body and many-body states of unitary bosons, $n(\mathbf{k})$ has subleading oscillations around the C_2/k^4 asymptotic tail. These consist in a log-periodic function of k, modulated by C_3/k^5 [25,35]. The three-body contact parameter C_3 vanishes at the length scale of the short-range hyperradial repulsion between atoms, induced by the van

der Waals potential [14] or by the explicit hyperradial cutoff R_0. Thus the subleading oscillations can, in our model, only be observed for $k \lesssim 1/R_0$. For our high-temperature results [cf. Fig. 3(e)], the asymptotic tail of $n(\mathbf{k})$ kicks in at $k > 1/R_0$, where C_3 is effectively zero, and we do not expect visible subleading corrections. At low temperature, however, the crossover into the asymptotic tail is at $k \approx 1/R_0$ [see Fig. 4(a)]. Thus, the subleading oscillations are possibly observable within the three-body-cutoff model, for a slightly smaller value of T or R_0, despite being beyond the current resolution.

In conclusion, we have computed the equilibrium phase diagram and the momentum distribution of the unitary Bose gas from first principles, overcoming the technical challenges through a novel quantum Monte Carlo algorithm [15]. Our theoretical predictions will most easily be checked in the currently available homogeneous traps [36,37], which are less subject to three-body losses than the traditional harmonic traps. In the near future, we expect high-precision experimental measurements of the superfluid transition and of the momentum distribution $n(\mathbf{k})$ in the unitary Bose gas.

We thank Riccardo Rossi for insightful suggestions, and acknowledge extensive discussions with Kris van Houcke, Xavier Leyronas, and Félix Werner. We thank Yvan Castin and Eric Cornell for discussions, and for allowing us reuse of data in Ref. [25] and in Ref. [13]. This work was performed in part at the Aspen Center for Physics, which is supported by National Science Foundation Grant No. PHY-1066293. This work was granted access to the HPC resources of MesoPSL financed by the Region Ile de France and the project Equip@Meso (reference ANR-10-EQPX-29-01) of the programme Investissements d'Avenir supervised by the Agence Nationale pour la Recherche.

*tommaso.comparin@ens.fr
†werner.krauth@ens.fr

[1] V. Efimov, Phys. Lett. B **33**, 563 (1970).
[2] T. Kraemer, M. Mark, P. Waldburger, J. G. Danzl, C. Chin, B. Engeser, A. D. Lange, K. Pilch, A. Jaakkola, H.-C. Nägerl, and R. Grimm, Nature (London) **440**, 315 (2006).
[3] C. Chin, R. Grimm, P. Julienne, and E. Tiesinga, Rev. Mod. Phys. **82**, 1225 (2010).
[4] E. Braaten and H.-W. Hammer, Phys. Rep. **428**, 259 (2006).
[5] G. Barontini, C. Weber, F. Rabatti, J. Catani, G. Thalhammer, M. Inguscio, and F. Minardi, Phys. Rev. Lett. **103**, 043201 (2009).
[6] J. R. Williams, E. L. Hazlett, J. H. Huckans, R. W. Stites, Y. Zhang, and K. M. O'Hara, Phys. Rev. Lett. **103**, 130404 (2009).
[7] R. Pires, J. Ulmanis, S. Häfner, M. Repp, A. Arias, E. D. Kuhnle, and M. Weidemüller, Phys. Rev. Lett. **112**, 250404 (2014).
[8] T. D. Lee, K. Huang, and C. N. Yang, Phys. Rev. **106**, 1135 (1957).
[9] Y. Castin and F. Werner, Can. J. Phys. **91**, 382 (2013) [English version arXiv:1212.5512].
[10] B. S. Rem, A. T. Grier, I. Ferrier-Barbut, U. Eismann, T. Langen, N. Navon, L. Khaykovich, F. Werner, D. S. Petrov, F. Chevy, and C. Salomon, Phys. Rev. Lett. **110**, 163202 (2013).
[11] R. J. Fletcher, A. L. Gaunt, N. Navon, R. P. Smith, and Z. Hadzibabic, Phys. Rev. Lett. **111**, 125303 (2013).
[12] U. Eismann, L. Khaykovich, S. Laurent, I. Ferrier-Barbut, B. S. Rem, A. T. Grier, M. Delehaye, F. Chevy, C. Salomon, L.-C. Ha, and C. Chin, Phys. Rev. X **6**, 021025 (2016).
[13] P. Makotyn, C. E. Klauss, D. L. Goldberger, E. A. Cornell, and D. S. Jin, Nat. Phys. **10**, 116 (2014).
[14] J. Wang, J. P. D'Incao, B. D. Esry, and C. H. Greene, Phys. Rev. Lett. **108**, 263001 (2012).
[15] T. Comparin and W. Krauth (to be published).
[16] S. Tan, Ann. Phys. (Amsterdam) **323**, 2952 (2008).
[17] F. Werner and Y. Castin, Phys. Rev. A **86**, 053633 (2012).
[18] D. M. Ceperley, Rev. Mod. Phys. **67**, 279 (1995).
[19] W. Krauth, Phys. Rev. Lett. **77**, 3695 (1996).
[20] M. Boninsegni, N. V. Prokof'ev, and B. V. Svistunov, Phys. Rev. E **74**, 036701 (2006).
[21] E. L. Pollock and D. M. Ceperley, Phys. Rev. B **36**, 8343 (1987).
[22] See Supplemental Material at http://link.aps.org/supplemental/10.1103/PhysRevLett.117.225301 for (i) the description of the $n(\mathbf{k})$ estimator, (ii) the study of c_2 at low temperature, (iii) more details on the superfluid transition, (iv) a comparison with the momentum distribution of noninteracting bosons, and (v) the analytical model for the gas-liquid coexistence.
[23] S. Piatecki and W. Krauth, Nat. Commun. **5**, 3503 (2014).
[24] Y. Yan and D. Blume, Phys. Rev. A **91**, 043607 (2015).
[25] Y. Castin and F. Werner, Phys. Rev. A **83**, 063614 (2011).
[26] J. von Stecher, J. Phys. B **43**, 101002 (2010).
[27] D. H. Smith, E. Braaten, D. Kang, and L. Platter, Phys. Rev. Lett. **112**, 110402 (2014).
[28] M. Barth and J. Hofmann, Phys. Rev. A **92**, 062716 (2015).
[29] X.-J. Liu, B. Mulkerin, L. He, and H. Hu, Phys. Rev. A **91**, 043631 (2015).
[30] J. M. Diederix, T. C. F. van Heijst, and H. T. C. Stoof, Phys. Rev. A **84**, 033618 (2011).
[31] M. Rossi, L. Salasnich, F. Ancilotto, and F. Toigo, Phys. Rev. A **89**, 041602 (2014).
[32] A. G. Sykes, J. P. Corson, J. P. D'Incao, A. P. Koller, C. H. Greene, A. M. Rey, K. R. A. Hazzard, and J. L. Bohn, Phys. Rev. A **89**, 021601 (2014).
[33] E. L. Pollock and K. J. Runge, Phys. Rev. B **46**, 3535 (1992).
[34] L. P. Pitaevskii and S. Stringari, *Bose-Einstein Condensation* (Oxford University Press, Oxford, 2003).
[35] E. Braaten, D. Kang, and L. Platter, Phys. Rev. Lett. **106**, 153005 (2011).
[36] A. L. Gaunt, T. F. Schmidutz, I. Gotlibovych, R. P. Smith, and Z. Hadzibabic, Phys. Rev. Lett. **110**, 200406 (2013).
[37] N. Navon, A. L. Gaunt, R. P. Smith, and Z. Hadzibabic, Science **347**, 167 (2015).